The Astrophysical Journal, 665:402–415, 2007 August 10

COHERENCE AND INTERMITTENCY OF ELECTRON DENSITY IN SMALL-SCALE INTERSTELLAR TURBULENCE

P. W. Terry and K. W. Smith
Center for Magnetic Self-Organization in Laboratory and Astrophysical Plasmas and Department of Physics, University of Wisconsin–Madison, Madison, WI 53706; pwterry@wisc.edu
Received 2006 December 14; accepted 2007 April 19

ABSTRACT

Spatial intermittency in decaying kinetic Alfvén wave turbulence is investigated to determine if it produces non-Gaussian density fluctuations in the interstellar medium. Non-Gaussian density fluctuations have been inferred from pulsar scintillation scaling. Kinetic Alfvén wave turbulence characterizes density evolution in magnetic turbulence at scales near the ion gyroradius. It is shown that intense localized current filaments in the tail of an initially Gaussian probability distribution function possess a sheared magnetic field that strongly refracts the random kinetic Alfvén waves responsible for turbulent decorrelation. The refraction localizes turbulence to the filament periphery, and hence it avoids mixing by the turbulence. As the turbulence decays, these long-lived filaments create a non-Gaussian tail. A condition related to the shear of the filament field determines which fluctuations become coherent and which decay as random fluctuations. The refraction also creates coherent structures in electron density. These structures are not localized. Their spatial envelope maps into a probability distribution that decays as density to the power -3. The spatial envelope of density yields a Levy distribution in the density gradient.

Subject headings: ISM: general — MHD — turbulence

1. INTRODUCTION

Pulasr radio signals probe fluctuations in the local interstellar medium (Armstrong et al. 1981). The broad electron density fluctuation spectrum (Armstrong et al. 1995) is commonly interpreted as a turbulent inertial range. The pulsar signal width yields information about fluctuation statistics (Bhat et al. 2004; Sutton 1971). The width scales as R^4 (R is the distance to the source), a result that is incompatible with Gaussian statistics (Boldyrev & Gwinn 2003b). The latter would produce a scaling of R^2, while R^4 is recovered for Levy statistics (Boldyrev & Gwinn 2003a). A Levy-distributed random walk typically consists of a series of small random steps punctuated by occasional Levy flights in which there is a single large jump to a new locale. In the context of a pulsar radio signal propagating through a Levy distribution of electron density fluctuations, a sea of low-intensity density fluctuations would scatter the signal through a series of small angles. Intermittently, as the signal traversed an intense, localized density fluctuation, it would scatter through a much larger angle.

The assertion that pulsar signals are dispersed by Levy-distributed fluctuations is a statistical *Ansatz* validated to some degree by observation. This *Ansatz* does not address the difficult and important question of what processes or conditions produce the statistics. It has been suggested that Levy statistics can emerge from radio signal trajectories grazing the surface of molecular clouds (Boldyrev & Königl 2006). Here we examine a different mechanism rooted in the turbulent cascade implied by the broad fluctuation spectrum. The mechanism is intrinsic spatial intermittency, a process known to create non-Gaussian tails in the probability distribution function (PDF). In Navier-Stokes turbulence, intrinsic intermittency takes the form of randomly dispersed, localized vortex strands, surrounded by regions of relative inactivity (Kerr 1986). Intermittency is most pronounced at small scales. Intermittency also occurs in MHD turbulence (Grappin et al. 1991). However, the statistical properties of electron density fluctuations in magnetic turbulence are not known. In this paper, we address the fundamental and nontrivial question of whether electron density can become intermittent in the magnetic turbulence of the interstellar medium (ISM). The effect on pulse-width scaling requires that additional issues be addressed, and these will be taken up later.

The question of intermittency in pulsar scintillation is twofold. First, can intermittent electron density fluctuations in interstellar turbulence achieve the requisite intensity to change the PDF? To some extent, this question has been answered by studies that show that passive advection and the limitations it places on electron density excitation (as indicated, e.g., by mixing-length arguments) applies only to scales larger than tens of gyroradii. At smaller scales, the electron density becomes active through kinetic Alfvén wave (KAW) interactions with magnetic fluctuations, exciting the internal energy to equipartition with the magnetic energy (Terry et al. 2001). Evidence for a transition to KAW dynamics near the gyroradius scale has recently been inferred from solar wind observations (Bale et al. 2005). Since scintillation is dominated by small scales, the regime of kinetic Alfvén interactions is appropriate for studying the intermittency potentially associated with the scaling of the pulsar signal width. The second aspect of intermittency in the context of pulsar signals deals with how isolated structures can form against the homogenizing influence of turbulent mixing in a type of turbulence that does not involve flow. Virtually all mechanisms proposed for intermittency involve flow or momentum, yet the flow of ions in magnetic turbulence decouples from small-scale kinetic Alfvén waves, with the interaction of magnetic field and density taking place against a background of unresponsive ions.

While intermittency has been widely studied in hydrodynamic turbulence (Frisch 1995) and MHD (Politano & Pouquet 1995), historically the emphasis has been on structure and statistics, not mechanisms. Structure studies have included efforts to visualize intermittent structures (Head & Bandyopadhyay 1981). Quantitatively, measurements of structure function scalings have been made to

gauge how intermittency changes with scale (She & Lévêque 1994; Politano & Pouquet 1995). Statistical characterizations of intermittency generally postulate a non-Gaussian statistical *Ansatz*, and the resultant properties are compared with measurements to determine if the *Ansatz* is reasonable. These approaches do not address the mechanisms that endow certain fluctuation structures either with individual longevity or collective prominence, in a statistical sense, relative to other regions in which such structures are not present (Waleffe 1997). The mechanistic approach is nascent but has already yielded significant insights into the long-standing problem of subcritical instability in plane Pouseuille flow (Hof et al. 2004).

A starting point for our considerations is simulations of decaying KAW turbulence that show the emergence of coherent, long-lived current filaments under collisional dissipation of density (Craddock et al. 1991). In these simulations, finite-amplitude fluctuations in density and magnetic field decayed from initial Gaussian distributions. (The current, as the curl of the magnetic field, was also Gaussian initially.) The distribution of current became highly non-Gaussian as certain current fluctuations persisted in the decay long past the nominal turbulent correlation time. The longevity of these filaments enhanced the tail of the PDF, steadily increasing the value of the fourth-order moment (kurtosis) significantly above its Gaussian value. While the PDF was affected by mutual interactions of filaments later in the simulation, initially the tail enhancement was dominated by the interaction of filaments with surrounding turbulence and the lack of mixing of those filaments relative to the rapidly decaying surrounding turbulence. Intermittency was not reported when resistivity dominated the dissipation. While these simulations showed intermittency in KAW turbulence, non-Gaussian statistics was demonstrated for current fluctuations, not density. The turbulence decayed by means of collisional dissipation of density; the current had no direct damping. It is not clear what effect this had on density structure formation within the constraints of the resolution of the simulations. The question of intermittency in density therefore remains open. No mechanism for the intermittency was proposed.

In this paper, we examine analytically the dynamics of structures in density and current and determine how one relates to the other. We will use analysis tools and results developed to understand the emergence of long-lived vortices in decaying two-dimensional (2D) Navier-Stokes turbulence (McWilliams 1984). For that problem, two-timescale analysis showed that the vortices are coherent and long-lived because strong shear flow in the outer part of the vortex suppresses ambient mixing by turbulence (Terry 1989; Terry et al. 1992). The ambient mixing would otherwise destroy the vortex in a turnover time. This mechanism for maintaining the coherent vortex in decaying turbulence correctly predicts the observed distribution of Gaussian curvature of the flow field (Terry 2000).

We use two-timescale analysis to describe coherent structure formation in decaying KAW turbulence. The following are obtained: (1) We identify the mechanism that allows certain current filaments to escape the turbulent mixing that otherwise typifies the turbulence. Current and density are mixed by the random interaction of kinetic Alfvén waves. This process is disrupted in current filaments whose azimuthal field has an unusually large amount of transverse shear. This creates a strong refraction of turbulent kinetic Alfvén waves that localizes them to the periphery of the filament and restricts their ability to mix current and density. (2) We derive a shear threshold criterion based on this mechanism. It identifies which current filaments escape mixing and become coherent, or long-lived. The criterion relates to the Gaussian curvature of the magnetic field, providing a topological construct that maps the intermittency in a way analogous to the flow Gaussian curvature of decaying 2D Navier-Stokes turbulence. (3) We trace the relative effects of the refractive shear mechanism on current, magnetic field, density, and flux. The magnetic field and density have long-lived, localized fluctuation structures that coexist spatially with localized current filaments. However, the magnetic field extends beyond the localized current. Like the magnetic field of a line current, it falls off as r^{-1}. Because the density is equipartitioned with the magnetic field in KAW turbulence, a similar mantle is expected for the density. This mantle tends to prevent the density kurtosis from rising to values greatly above 3; however, it is responsible for giving the PDF of density gradient a Levy distribution.

This paper is organized as follows: Section 2 presents the kinetic Alfvén wave model used in this paper. The two-timescale analysis is introduced in § 3. Section 4 derives the condition for strong refraction, and the resultant refractive boundary-layer structure for turbulent KAW activity in and around the coherent filament. The turbulent mixing stresses are determined in § 5, from which the filament and density lifetimes can be derived. Section 6 discusses the Gaussian curvature and spatial properties of the current and density structures. The latter are used to infer heuristic PDFs. Conclusions are given in § 7.

2. KINETIC ALFVÉN WAVE MODEL

The shear Alfvén and kinetic Alfvén physics described in § 1 is intrinsic to models of MHD augmented by electron continuity. When there is a strong mean field, the nonlinear MHD dynamics can be represented with a reduced description (Hazeltine 1993), given by

$$\frac{\partial \hat{\psi}}{\partial t} + \nabla_{\parallel}\hat{\phi} = \eta \hat{J} + \nabla_{\parallel}\hat{n} + \frac{C_s}{V_{\rm A}}\frac{1}{n_0}\nabla\hat{\psi} \times \boldsymbol{z} \cdot \nabla n_0, \tag{1}$$

$$\frac{\partial}{\partial t}\nabla_{\perp}^2\hat{\phi} - \nabla\hat{\phi} \times \boldsymbol{z} \cdot \nabla\nabla_{\perp}^2\hat{\phi} = -\nabla_{\parallel}\hat{J}, \tag{2}$$

$$\frac{\partial \hat{n}}{\partial t} - \nabla\hat{\phi} \times \boldsymbol{z} \cdot \nabla\hat{n} + \nabla_{\parallel}\hat{J} - \frac{C_s}{V_{\rm A}}\frac{1}{n_0}\nabla\hat{\phi} \times \boldsymbol{z} \cdot \nabla n_0 = 0, \tag{3}$$

where

$$\nabla_{\parallel} = \frac{\partial}{\partial z} + \nabla\hat{\psi} \times \boldsymbol{z} \cdot \nabla \tag{4}$$

and $\hat{J} = \nabla_{\perp}^2\hat{\psi} = \partial^2\hat{\psi}/\partial x^2 + \partial^2\hat{\psi}/\partial y^2$. In the reduced description, the perturbed magnetic field is perpendicular to the mean field and can be written as $\hat{\boldsymbol{b}}/B = \nabla\hat{\psi} \times \boldsymbol{z}$, where $\boldsymbol{z}$ is the direction of the mean field and $\hat{\psi} = (C_s/c)eA_z/T_e$ is the normalized parallel component of the vector potential. The flow has zero mean and is also perpendicular to the mean field B. It can be expressed in terms of the electrostatic potential as $-\nabla\hat{\phi} \times \boldsymbol{z}$, where $\hat{\phi} = (C_s/V_{\rm A})e\phi/T_e$ is the normalized electrostatic potential. The normalized density fluctuation

is $\hat{n} = (C_s/V_A)\tilde{n}/n_0$, where n_0 is the mean density, and $\eta = (c^2/4\pi V_A \rho_s)\eta_{Sp}$ is the normalized resistivity, where η_{Sp} is the Spitzer resistivity. Spatial scales are normalized to $\rho_s = C_s/\Omega_i$, time is normalized to the Alfvén time $\tau_A = \rho_s/V_A$, $C_s = (T_e/m_i)^{1/2}$ is the ion acoustic velocity, $V_A = B/(4\pi m_i n_0)^{1/2}$ is the Alfvén velocity, and $\Omega_i = eB/m_i c$ is the ion gyrofrequency. Within their limitations (isothermal, incompressible fluctuations), equations (1)–(4) are valid for scales both large and small compared with the gyroradius, as well as the intermediate region.

Equation (3) is the electron continuity equation. The advective nonlinearity, $\nabla\hat{\phi} \times \boldsymbol{z} \cdot \nabla\hat{n}$, couples electron density fluctuations to the flow. If there is a nonuniform mean density, advection drives weak density fluctuations of amplitude $\hat{n} \approx (\delta/L_n)n_0$, where δ is the scale of density fluctuations and L_n is the mean density scale length. The continuity equation also contains a compressible nonlinearity, $\nabla_\parallel \hat{J}$, whereby compressible electron motion along magnetic field perturbations provides coupling to the magnetic field. Electrons act on the magnetic field through parallel electron pressure in Ohm's law, expressed as $\nabla_\parallel \hat{n}$ in equation (1). The couplings of magnetic field and density are weak at scales appreciably larger than the ion gyroradius. On those scales, the advection of electron density is passive to a good approximation and governs electron density evolution. In the region around $\delta = 10\rho_s$, the two nonlinearities in each of equations (1)–(3) become comparable (Terry et al. 2001). For $\delta < 10\rho_s$, $\nabla_\parallel \hat{n}$ begins to dominate $\nabla_\parallel \hat{\phi}$ in equation (1) and $\nabla_\parallel \hat{J}$ begins to dominate $\nabla\hat{\phi} \times \boldsymbol{z} \cdot \nabla\hat{n}$ in equation (3). This is a very different regime from incompressible MHD, where the magnetic field and flow actively exchange energy through shear Alfvén waves. In a turbulent cascade approaching the ion gyroradius scale from larger scales, the energy exchanged between flow and magnetic field in shear Alfvén interactions diminishes relative to the energy exchanged between the electron density and the magnetic field through the compressible coupling. Consequently, flow decouples from the magnetic field, increasingly evolving as a go-it-alone Kolmogorov cascade, while electron density and magnetic field, interacting compressively through kinetic Alfvén waves, supplant the shear Alfvén waves. Once the kinetic Alfvén wave coupling reaches prominence, the internal and magnetic energies become equipartitioned, $\int \hat{n}^2\, dV \approx \int |\nabla\hat{\psi}|^2 dV$, even if the internal energy is only a fraction of the magnetic energy at larger scales. If there is no significant damping at the ion gyroradius scale, the large-scale shear Alfvén cascade continues to gyroradius scales and beyond though kinetic Alfvén waves. The gyroradius scale at which KAW dynamics is active is on the order of 10^8 cm in the warm ISM. This is small relative to the scale of intermittent flow structures in molecular gas clouds, recently reported to be on the order of 10^{18} cm (Hily-Blant et al. 2007). This scale difference is crudely consistent with the high magnetic Prandtl number of the warm ISM. The value $\mathrm{Pr} \sim 10^{14}$ allows very small scales in the ionized medium, before dissipation becomes important, relative to scales of viscous dissipation in the clouds. The gyroradius scale of intermittent KAW structures makes direct visualization in the ISM difficult.

In the KAW regime, the model can be further simplified by dropping the flow evolution. This leaves a KAW model in which electron density and magnetic field interact against a neutralizing background of unresponsive ions,

$$\frac{\partial\hat{\psi}}{\partial t} = \frac{\partial\hat{n}}{\partial z} + \nabla\hat{\psi} \times \boldsymbol{z} \cdot \nabla\hat{n} + \eta\hat{J} + \frac{C_s}{V_A}\frac{1}{n_0}\nabla\hat{\psi} \times \boldsymbol{z} \cdot \nabla n_0, \tag{5}$$

$$\frac{\partial\hat{n}}{\partial t} + \frac{\partial\hat{J}}{\partial z} + \nabla\hat{\psi} \times \boldsymbol{z} \cdot \nabla\hat{J} - \mu\nabla^2\hat{n} = 0. \tag{6}$$

Solutions of this model closely approximate those of equations (1)–(3) when the scales are near the gyroradius or smaller (Terry et al. 1998). This model assumes isothermal fluctuations, consistent with strong parallel thermal conductivity. Equations (5) and (6) are fluid equations, and hence Landau-resonant (Howes et al. 2006) and gyroresonant dissipation, which may be important in the ISM, are not modeled. Ohm's law has resistive dissipation, and density evolution has collisional diffusion. Depending on the ratio η/μ, either of these dissipation mechanisms can damp the energy in decaying turbulence; however, the damping occurs at small dissipative scales. We will focus on inertial behavior at larger scales. We assume that mean density is nearly uniform and neglect the last term of equation (5).

The dispersion relation for ideal kinetic Alfvén waves is determined by linearizing equations (5) and (6), neglecting resistive dissipation $\eta\hat{J}$, and introducing a Fourier transform in space and time. The result is $\omega = k_z k_\perp$, where $\boldsymbol{k}_\perp \cdot \boldsymbol{z} = 0$, or $\boldsymbol{k}_\perp \perp k_z\boldsymbol{z}$. If dimensional frequency and wavenumbers $\tilde{\omega}$, $\tilde{k}_z$, and $\tilde{k}_\perp$ are reintroduced, the dispersion relation is $\tilde{\omega} = V_A \tilde{k}_z \tilde{k}_\perp \rho_s$. The wave can be seen to combine Alfvénic propagation with perpendicular motion associated with the gyroradius scale. The KAW eigenvector yields equal amplitudes of magnetic field and the density, $-k_\perp\psi_k = ib_k = n_k$, with a phase difference of $\pi/2$.

In magnetic turbulence, with its hierarchy of scales, kinetic Alfvén waves also propagate along components of the turbulent magnetic field. In the reduced description the turbulent field is perpendicular to the mean field, and hence the dispersion relation of these kinetic Alfvén waves carries no k_z-dependence. To illustrate, we isolate such a fluctuation from the mean field kinetic Alfvén wave by setting $k_z = 0$; with this wavenumber zero, we drop the subscript from $k_\perp$; we consider a turbulent magnetic field component $\hat{\boldsymbol{b}}_{k_0}/B_0 = i\boldsymbol{k}_0 \times \boldsymbol{z}\psi_{k_0}$ at wavenumber k_0 that dominates the low-k fluctuation spectrum; and we look at the dispersion for smaller scale fluctuations satisfying $k \gg k_0$. The latter conditions linearize the problem, yielding a dispersion relation for kinetic Alfvén waves propagating along the turbulent field $\hat{\boldsymbol{b}}_{k_0}$ according to $\omega = i\boldsymbol{k}_0 \times \boldsymbol{z} \cdot \boldsymbol{k}\psi_{k_0}k = (\hat{\boldsymbol{b}}_{k_0} \cdot \boldsymbol{k}/B)k$. Reintroducing dimensions, $\tilde{\omega} = V_A(\boldsymbol{b}_{k_0} \cdot \tilde{\boldsymbol{k}}/B)\tilde{k}\rho_s$. One can see that the dispersion is Alfvénic, but with respect to a perturbed field component that is perpendicular to the mean field. Hence the frequency varies as $\tilde{k}^2\rho_s$ instead of $\tilde{k}_z\tilde{k}\rho_s$.

3. TWO-TIMESCALE ANALYSIS

To understand and quantify the conditions under which a coherent current fluctuation persists for long times relative to typical fluctuations, we examine the interaction of the coherent structure with surrounding turbulence and derive its lifetime under turbulent mixing. The interaction is described using a two-timescale analysis, allowing evolution on disparate timescales to be tracked (Terry et al. 1992). The coherent structure, a current filament with accompanying magnetic field and electron density fluctuations, evolves on the slow timescale under the rapid-scale–averaged effect of turbulence. On the rapid scale the filament is essentially stationary, creating an inhomogeneous background for the rapidly evolving turbulence. Identifying conditions that support longevity justifies

the two-timescale approximation a posteriori. Simulations suggest the filament is roughly circular. If coordinates are chosen with the origin at the center of the filament, a circular filament is azimuthally symmetric, while the turbulence breaks that symmetry.

The filament current is localized, and hence its current density becomes zero at some distance from the origin. The localized current profile necessarily creates a magnetic field that is strongly inhomogeneous. On the rapid timescale over which the turbulence evolves, this field, which is part of the coherent structure, is essentially stationary. It acts as a secondary equilibrium field in addition to the primary equilibrium field (which is homogeneous and directed along the z-axis). Turbulence, in the form of random kinetic Alfvén waves, propagates along both the primary and secondary fields. Because the primary field is homogeneous, its effect on the turbulence is uninteresting. However, the secondary field is strongly sheared because of the local inhomogeneity created by the structure. Strong shear refracts the turbulent kinetic Alfvén waves. In the subsequent analysis we will ignore the primary KAW propagation, which we can do by setting $k_z = 0$, and focus on the refraction of KAW propagation by the secondary magnetic field shear. Strong refraction will be shown to localize kinetic Alfvén waves away from the heart of the filament, allowing it to escape mixing and thereby acquire the longevity to make it coherent.

With $J = \nabla_\perp^2 \hat{\psi}$, we apply the separation of long and short timescales to fluctuations in $\hat{n}$ and $\hat{\psi}$ as follows:

$$\hat{F} = F_0(r, \tau) + \tilde{F}(r, \theta, t), \tag{7}$$

where the symbol F represents either ψ or n, with ψ_0 and n_0 the flux function and density of the coherent structure and $\tilde{\psi}$ and $\tilde{n}$ the turbulent fields of flux and density. The variables for slowly and rapidly evolving time are τ and t. The origin of a polar coordinate system with radial and angle variables r and θ is placed at the center of the structure. The structure is assumed to be azimuthally symmetric. The turbulence evolves in the presence of the structure, and hence it is necessary to specify the radial profile of ψ_0 or, more explicitly, the profile of the secondary, structure field $\nabla\psi_0(r) \times \hat{z} = B_\theta(r)\hat{\boldsymbol{\theta}}$. As a generic profile for localized current, we adopt a reference profile that peaks at the origin and falls monotonically to zero over a finite radius a. For simplicity we take the variation to be quadratic, giving

$$J_0(r) = J_0(0)\left(1 - \frac{r^2}{a^2}\right), \tag{8}$$

where $J_0(r) = \partial^2\psi_0/\partial r^2$. Integrating the current, we obtain

$$B_\theta(r) = \begin{cases} \dfrac{J_0(0)}{2} r\left(1 - \dfrac{r^2}{2a^2}\right), & \text{for } r \le a, \\ \dfrac{J_0(0)a^2}{4r}, & \text{for } r \ge a. \end{cases} \tag{9}$$

These profiles are for reference. Shortly we will introduce a more general description for a filament whose current peaks at the origin and decays monotonically. The current of the coherent filament is wholly localized within $r = a$. However, the magnetic field is not localized but slowly decays as r^{-1} outside the filament. The quantities in equations (8)–(9) all evolve on the slow timescale τ. The dependence on τ is not notated, because when B_θ appears in the turbulence equations it is a quasi-equilibrium quantity on the rapid timescale.

To describe the rapid-timescale evolution and its azimuthal variations we introduce a Fourier-Laplace transform,

$$\tilde{F}(r, \theta, t) = \frac{1}{2\pi i}\int_{-i\infty+\gamma_0}^{+i\infty+\gamma_0} d\gamma \sum_m \tilde{F}_{m,\gamma}(r) \exp(-im\theta) \exp \gamma t, \tag{10}$$

where γ_0 is the shift of the complex integration path of the inverse Laplace transform. The radial variation of $B_\theta(r)$ creates an inhomogeneous background field for the turbulence, making Fourier transformation unsuitable for the radial variable. The Laplace transform is appropriate for turbulence that decays from an initial state. To obtain equations for the slowly evolving fields ψ_0 and n_0, we average the full equations over the rapid timescale t. This is accomplished by applying the Laplace transform to the equations and integrating over t. The integral selects $\gamma = 0$ as the time average, that is, $\int dt\, f(\tau, t) = \int dt \int d\gamma (2\pi i)^{-1} f_\gamma(\tau) \exp \gamma t = f_{\gamma=0}(\tau)$. Applying this procedure, the evolution equations for the slowly evolving fields are given by

$$\frac{\partial \psi_{\gamma=0}(\tau)}{\partial \tau} - \frac{1}{2\pi i}\int_{-i\infty+\gamma_0}^{+i\infty+\gamma_0} d\gamma' \sum_{m'} \left\langle \left[\tilde{b}_{r(-m',-\gamma')}\frac{\partial}{\partial r} + \tilde{b}_{\theta(-m',-\gamma')}\left(\frac{im'}{r}\right)\right]\tilde{n}_{m',\gamma'}\right\rangle = 0, \tag{11}$$

$$\frac{\partial n_{\gamma=0}(\tau)}{\partial \tau} + \frac{1}{2\pi i}\int_{-i\infty+\gamma_0}^{+i\infty+\gamma_0} d\gamma' \sum_{m'} \left\langle \left[\tilde{b}_{r(-m',-\gamma')}\frac{\partial}{\partial r} + \tilde{b}_{\theta(-m',-\gamma')}\left(\frac{im'}{r}\right)\right]\left[\frac{1}{r}\frac{\partial}{\partial r}\left(r\frac{\partial}{\partial r}\right) - \frac{m'^2}{r^2}\right]\tilde{\psi}_{m',\gamma'}\right\rangle = 0, \tag{12}$$

where $\tilde{b}_{r(-m',-\gamma')}$, $\tilde{b}_{\theta(-m',-\gamma')}$, $n_{m',\gamma'}$, and $\tilde{\psi}_{m',\gamma'}$ are understood to depend on the radial variable r; $\tilde{b}_{r(-m',-\gamma')} = (-im'/r)\psi_{-m',-\gamma'}$ and $\tilde{b}_{\theta(-m',-\gamma')} = -(\partial/\partial r)\psi_{-m',-\gamma'}$. The correlations $\langle \tilde{b}_r \partial\tilde{n}/\partial r\rangle$, $\langle \tilde{b}_\theta \tilde{n}\rangle$, $\langle \tilde{b}_r \partial\nabla^2\tilde{\psi}/\partial r\rangle$, and $\langle \tilde{b}_\theta \nabla^2\tilde{\psi}\rangle$, which appear in equations (11) and (12), are turbulent stresses associated with random kinetic Alfvén wave refraction. Their fast time averages govern the mixing (transport) of the coherent fields. These stresses must be evaluated from solutions of the fast-timescale equations to find the lifetime of the structure.

The evolution equations for the rapidly evolving turbulent fluctuations are

$$\gamma\tilde{\psi}_{m,\gamma} - B_\theta(r)\left(\frac{-im}{r}\right)\tilde{n}_{m,\gamma} + \frac{1}{2\pi i}\int_{-i\infty+\gamma_0}^{+i\infty+\gamma_0} d\gamma' \sum_{m'}\left[\frac{im'}{r}\tilde{\psi}_{m',\gamma'}\frac{\partial}{\partial r} - \frac{i(m-m')}{r}\frac{\partial\tilde{\psi}_{m',\gamma'}}{\partial r}\right]\tilde{n}_{m-m',\gamma-\gamma'} = \frac{im}{r}\tilde{\psi}_{m,\gamma}\frac{\partial}{\partial r}n_0(r), \tag{13}$$

$$\begin{aligned}\gamma\tilde{n}_{m,\gamma} - B_\theta(r)\left(\frac{-im}{r}\right)&\left[\frac{1}{r}\frac{\partial}{\partial r}\left(r\frac{\partial}{\partial r}\right) - \frac{m^2}{r^2}\right]\tilde{\psi}_{m,\gamma} \\ &- \frac{1}{2\pi i}\int_{-i\infty+\gamma_0}^{+i\infty+\gamma_0} d\gamma' \sum_{m'}\left[\frac{im'}{r}\tilde{\psi}_{m',\gamma'}\frac{\partial}{\partial r} - \frac{i(m-m')}{r}\frac{\partial\tilde{\psi}_{m',\gamma'}}{\partial r}\right]\left[\frac{1}{r}\frac{\partial}{\partial r}\left(r\frac{\partial}{\partial r}\right) - \frac{(m-m')^2}{r^2}\right]\tilde{\psi}_{m-m',\gamma-\gamma'} \\ &= \frac{im}{r}\tilde{\psi}_{m,\gamma}\frac{\partial}{\partial r}J_0(r).\end{aligned} \tag{14}$$

We have not shown the dissipative terms, in accordance with our focus on inertial scales. The sources contain gradients of $n_0(r)$ and $J_0(r)$. These are the density and current of the coherent structure but, unlike $\psi_{\gamma=0}(\tau)$ and $n_{\gamma=0}(\tau)$, are not evaluated in the Laplace-transform domain. Three terms drive the evolution of $\partial\hat{\psi}/\partial t$ and $\partial\hat{n}/\partial t$ in each of these equations. The first term describes linear kinetic Alfvén wave propagation along the inhomogeneous secondary magnetic field B_θ of the coherent structure. The second term is the nonlinearity and describes turbulence of random kinetic Alfvén waves. The third term is proportional to mean field gradients. It is a fluctuation source via the magnetic analog of advection ($\nabla\hat{\phi}\times\hat{\boldsymbol{z}}\cdot\nabla = \boldsymbol{v}\cdot\nabla \rightarrow \nabla\hat{\psi}\times\hat{\boldsymbol{z}}\cdot\nabla$). It yields quasi-linear diffusivities for the turbulent mixing process. For example, if the kinetic Alfvén wave and nonlinear terms of equation (14) are dropped, the solution is

$$\tilde{n}^{(i)}_{m,\gamma} = \frac{1}{\gamma}\frac{im}{r}\tilde{\psi}_{m,\gamma}\frac{\partial J_0(r)}{\partial r}. \tag{15}$$

The superscript (i) indicates that for deriving diffusivities, this density is to be substituted iteratively into the correlations of the turbulent stresses. From equation (11) these correlations are $\langle\tilde{b}_r\tilde{n}\rangle = \langle\tilde{b}^{(i)}_r\tilde{n}\rangle + \langle\tilde{b}_r\tilde{n}^{(i)}\rangle$ and $\langle\tilde{b}_\theta\partial\tilde{n}/\partial r\rangle = \langle\tilde{b}^{(i)}_\theta\partial\tilde{n}/\partial r\rangle + \langle\tilde{b}_\theta\partial\tilde{n}^{(i)}/\partial r\rangle$. Substitution of equation (15) yields mean turbulent diffusivities for ψ_0. Similarly, if equation (13) is solved by dropping its kinetic Alfvén wave and nonlinear terms, we obtain

$$\tilde{\psi}^{(i)}_{m,\gamma} = \frac{1}{\gamma}\frac{im}{r}\tilde{\psi}_{m,\gamma}\frac{\partial n_0(r)}{\partial r}. \tag{16}$$

Substituting this solution into the correlations $\langle\tilde{b}_r\nabla^2\tilde{\psi}\rangle = \langle\tilde{b}^{(i)}_r\nabla^2\tilde{\psi}\rangle + \langle\tilde{b}_r\nabla^2\tilde{\psi}^{(i)}\rangle$ and $\langle\tilde{b}_\theta\partial\nabla^2\tilde{\psi}/\partial r\rangle = \langle\tilde{b}^{(i)}_\theta\partial\nabla^2\tilde{\psi}/\partial r\rangle + \langle\tilde{b}_\theta\partial\nabla^2\tilde{\psi}^{(i)}/\partial r\rangle$ of equation (12), mean turbulent diffusivities are obtained for n_0. Off-diagonal transport (relaxation of ψ_0 by the gradient of n_0) can also be obtained by substituting equation (16) into $\langle\tilde{b}_r\tilde{n}\rangle$ and $\langle\tilde{b}_\theta\partial\tilde{n}/\partial r\rangle$. The role of the nonlinear and kinetic Alfvén wave terms omitted from equations (15) and (16) is to modify the timescale γ and couple the sources. This is calculated in the next section. The inverse of γ represents the lifetime of the correlations $\langle\tilde{b}_r\tilde{n}\rangle$, $\langle\tilde{b}_\theta\partial\tilde{n}/\partial r\rangle$, $\langle\tilde{b}_r\nabla^2\tilde{\psi}\rangle$, and $\langle\tilde{b}_\theta\partial\nabla^2\tilde{\psi}/\partial r\rangle$. Generally, the nonlinear terms enhance decorrelation, increasing the effective value of γ. If the shear in B_θ is strong, the kinetic Alfvén wave term increases γ even further.

The role of shear in the kinetic Alfvén wave terms is not explicit but should be, so that it can be varied independently of the field amplitude $B_\theta(r_0)$ at some radial location r_0. In explicitly displaying the role of shear we note that if $B_\theta(r) \sim r$, as would be true if the current density J_0 were uniform, the kinetic Alfvén wave term is independent of r. In this situation the phase fronts of kinetic Alfvén waves propagating along B_θ are straight-line rays extending from the origin. Shear in B_θ, occurring through nonuniformity of J_0, distorts the phase fronts, as shown in Figure 1. Distortion occurs if B_θ has a variation that is not linear. From equation (9) we note that the variation of B_θ for our chosen structure profile is linear for $r \ll a$, with variations developing as $r \rightarrow a$. Therefore, it makes sense to quantify the shear by expanding $B_\theta(r)/r$ in a Taylor series about some point of interest. Obviously, the shear is zero at the origin and becomes sizable as $r \rightarrow$ a. Expanding about a reference point r_0 away from the origin,

$$\frac{B_\theta(r)}{r} = \frac{B_\theta(r_0)}{r_0} + (r-r_0)\frac{d}{dr}\left(\frac{B_\theta}{r}\right)\bigg|_{r_0} + \cdots. \tag{17}$$

If $B_\theta(r)$ varies smoothly, as is the case for a monotonically decreasing current profile, we can truncate the expansion as indicated in equation (17) and use that expression as a general current profile. Looking at the kinetic Alfvén terms of equations (13) and (14), the first term will produce a uniform frequency that effectively Doppler-shifts γ by the amount $imB_\theta(r_0)/r_0$. The second term will describe KAW propagation in an inhomogeneous medium with its attendant refraction.

4. REFRACTION BOUNDARY LAYER

We rewrite equation (14), substituting the expansion of equation (17), yielding

$$\begin{aligned}\gamma\tilde{n}_{m,\gamma} + \hat{\gamma}\nabla^2_m\tilde{\psi}_{m,\gamma} - im(r-r_0)\frac{d}{dr}\left(\frac{B_\theta}{r}\right)\bigg|_{r_0}\nabla^2_m\tilde{\psi}_{m,\gamma} \\ - \frac{1}{2\pi i}\int_{-i\infty+\gamma_0}^{+i\infty+\gamma_0} d\gamma' \sum_{m'}\left[\frac{im'}{r}\tilde{\psi}_{m',\gamma'}\frac{\partial}{\partial r} - \frac{i(m-m')}{r}\frac{\partial\tilde{\psi}_{m',\gamma'}}{\partial r}\right]\nabla^2_{m-m'}\tilde{\psi}_{m-m',\gamma-\gamma'} = \frac{im}{r}\tilde{\psi}_{m,\gamma}\frac{\partial}{\partial r}J_0(r),\end{aligned} \tag{18}$$

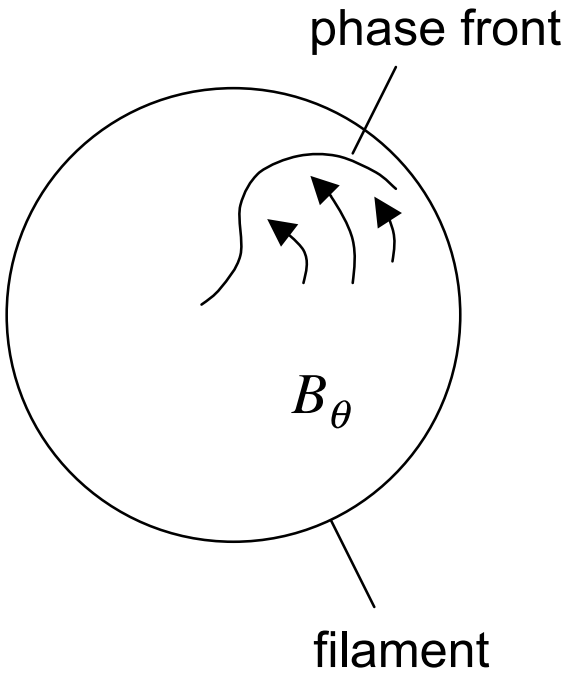

FIG. 1.—Distortion of a kinetic Alfvén wave phase front by a sheared filament field.

where

$$\nabla_m^2 = \frac{1}{r}\frac{\partial}{\partial r}\left(r\frac{\partial}{\partial r}\right) - \frac{m^2}{r^2} \tag{19}$$

and $\hat{\gamma} = imB_\theta(r_0)/r_0$. When $d/dr(B_\theta/r)|_{r_0}$ is large, the shear in B_θ refracts turbulent KAW activity. The process can be described using asymptotic analysis. In the limit that $d/dr(B_\theta/r)|_{r_0}$ becomes large asymptotically, the higher derivative nonlinear term is unable to remain in the dominant asymptotic balance unless the solution develops a small-scale boundary-layer structure. The layer is a singular structure. Its width must become smaller as $d/dr(B_\theta/r)|_{r_0}$ becomes larger, otherwise the highest-order derivative drops out of the balance and the equation changes order. This is the only viable asymptotic balance for $d/dr(B_\theta/r)|_{r_0} \to \infty$. The boundary layer's width Δr is readily estimated from dimensional analysis by noting that $r - r_0 \sim \Delta r$ and $\partial\nabla_m^2\tilde{\psi}_m(t)/\partial r \sim \nabla_m^2\tilde{\psi}_m/\Delta r$ and treating $d/dr(B_\theta/r)|_{r_0} \equiv j'$ as the diverging asymptotic parameter. The asymptotic balance is

$$\Delta r j' \nabla_m^2\tilde{\psi}_m(t) \sim \frac{1}{a}\tilde{\psi}_m(t)\frac{\nabla_m^2\tilde{\psi}_m(t)}{\Delta r} \qquad (j' \to \infty), \tag{20}$$

yielding

$$\Delta r \sim \sqrt{\tilde{\psi}_m/aj'} \qquad (j' \to \infty). \tag{21}$$

The length Δr is the scale of fluctuation variation within the coherent current filament. In the simulations, the filaments were identified as regions of strong, localized, symmetric current surrounded by turbulent fluctuations. Consequently, Δr represents a fluctuation penetration depth into the structure. We derived the layer width Δr from linear and nonlinear kinetic Alfvén wave terms operating on flux in the density equation. Identical operators apply to n in the flux equation. Hence, Δr is the width of a single layer pertaining to both the density and current fluctuations of refracted KAW turbulence. This structure is shown schematically in Figure 2. The above analysis indicates a single layer width and gives its value. It does not give the functional variation of current and density fluctuations within the layer, either relative or absolute.

In the simpler case of intermittency in decaying 2D Navier-Stokes turbulence, statistical closure theory was used to derive spatial functions describing the inhomogeneity of turbulence in the presence of a coherent vortex (Terry et al. 1992). There, coherent vortices suppress turbulent penetration by means of strong shear flow, analogous to the role of refraction here. For the KAW system, the closure equations are much more complicated and not amenable to the WKB analysis that gave the functional form of the boundary layer in the Navier-Stokes case. However, the closure remains useful. It provides a mathematical platform from which to calculate all aspects of the interaction of filament and turbulence, including the accelerated decay of turbulence within the boundary layer, the spatial characteristics of the layer, and the amplitudes of n and ψ. These are necessary for calculating turbulent mixing rates of the filament current and density.

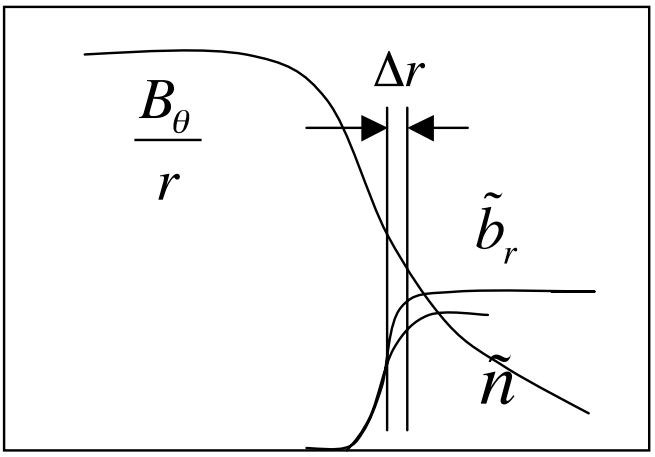

FIG. 2.—Boundary layer at edge of filament (just inside $r = a$). External fluctuations rapidly decay across the layer.

Closures can be applied to intermittent turbulence even though they rely on Gaussian statistics. The filaments, which make the system non-Gaussian as a whole, are quasi-stationary on the short timescale of turbulent evolution. Therefore, on that scale their only effect is to make the turbulence inhomogeneous. The fast-timescale statistics are a property of fast-timescale nonlinearity and remain Gaussian. The closure equations are

$$\hat{\gamma}\tilde{\psi}_{m,\gamma} - im(r-r_0)j'\tilde{n}_{m,\gamma} - D_{\psi\psi}(m,\gamma)\frac{\partial^2}{\partial r^2}\nabla^2\tilde{\psi}_{m,\gamma} - D_{\psi n}(m,\gamma)\frac{\partial^2}{\partial r^2}\tilde{n}_{m,\gamma} = \frac{im}{r}\tilde{\psi}_{m,\gamma}\frac{d}{dr}n_0(r), \tag{22}$$

$$\hat{\gamma}\tilde{n}_{m,\gamma} - im(r-r_0)j'\nabla^2\tilde{\psi}_{m,\gamma} - D^{(1)}_{n\psi}(m,\gamma)\frac{\partial^2}{\partial r^2}\nabla^2\tilde{\psi}_{m,\gamma} - D^{(2)}_{n\psi}(m,\gamma)\frac{\partial^2}{\partial r^2}\nabla^4\tilde{\psi}_{m,\gamma}$$
$$- D^{(1)}_{nn}(m,\gamma)\frac{\partial^2}{\partial r^2}\nabla^2\tilde{n}_{m,\gamma} - D^{(2)}_{nn}(m,\gamma)\frac{\partial^2}{\partial r^2}\tilde{n}_{m,\gamma} = \frac{im}{r}\tilde{\psi}_{m,\gamma}\frac{d}{dr}J_0(r). \tag{23}$$

This system is complex. The six diffusivities all contribute to the lowest order as $j' \to \infty$. (The diffusion coefficients and derivatives are not of the same order, but their product is.) Moreover, there is varied dependence on fluctuation correlations, and there are complex turbulent decorrelation functions. For example,

$$D_{\psi\psi}(m,\gamma) = \frac{1}{2\pi i}\int_{-i\infty+\gamma_0}^{+i\infty+\gamma_0} d\gamma' \sum_{m'\neq 0,\,m}\frac{m'}{r}\left[\left\langle\tilde{\psi}_{m',\gamma'}P^{-1}_{m-m'}\Delta W_{\gamma,\gamma'}\frac{m'}{r}\psi_{-m',-\gamma'}\right\rangle\right.$$
$$\left. + K_1(m-m',\gamma-\gamma')P^{-1}_{m-m'}\Delta W_{\gamma,\gamma'}\langle\psi_{-m',-\gamma'}\tilde{n}_{m',\gamma'}\rangle\right], \tag{24}$$

where

$$P_m = \left\{-\left[-imj'(r-r_0)\nabla^2_m - D^{(1)}_{n\psi}(m,\gamma)\frac{\partial^2}{\partial r^2}\nabla^2_m - D^{(2)}_{n\psi}(m,\gamma)\frac{\partial^2}{\partial r^2}\nabla^4_m - \frac{im}{r}\frac{d}{dr}J_0\right]K_1(m,\gamma)\right.$$
$$\left. + \hat{\gamma} - D^{(1)}_{nn}(m,\gamma)\frac{\partial^2}{\partial r^2}\nabla^2_m - D^{(2)}_{nn}(m,\gamma)\frac{\partial^2}{\partial r^2}\right\}, \tag{25}$$

$$K_1(m,\gamma) = \left[-\hat{\gamma} + D_{\psi\psi}(m,\gamma)\frac{\partial^2}{\partial r^2}\nabla^2_m - \frac{im}{r}\frac{d}{dr}n_0\right]^{-1}\left[imj'(r-r_0) + D_{\psi n}(m,\gamma)\frac{\partial^2}{\partial r^2}\right], \tag{26}$$

and $\Delta W(\gamma, \gamma')$ is the decorrelation rate for fluctuations at γ' driving γ. Expressions for the other diffusivities are given in the Appendix. We now calculate turbulence properties from the closure equations.

4.1. *Decay Time for Turbulence in the Filament*

The timescale of turbulent evolution in the filament is given by $\hat{\gamma}$. As $j' \to \infty$, this is dominated by the refraction. Hence the first terms of equation (22) and equation (23) must balance the second terms, which in turn must balance the remaining nonlinear terms. If equations (22) and (23) are solved jointly retaining the first two terms, $\hat{\gamma} \sim im(r-r_0)j'\nabla$ as $j' \to \infty$. Because $(r-r_0) \sim \Delta r$ and $\nabla \sim 1/\Delta r$,

$$\hat{\gamma} \sim imj' \qquad (j' \to \infty). \tag{27}$$

This timescale is purely imaginary, that is, oscillatory, when derived from a balance with only the linear Alfvén terms. When the diffusivities are included, it is complex. This rapid decay suppresses turbulence in the filament relative to levels outside the filament.

4.2. *Alfvénic Boundary Layer Width*

The width Δr, as derived above, comes from independent balances in the equations for n and ψ and does not account for the kinetic Alfvén wave dynamics that links n and ψ. To do that, equations (22) and (23) are combined into a single equation by operating on equation (23) with $-im(r - r_0)j' - D_{\psi n}(m, \gamma)\partial^2/\partial r^2$ and substituting from equation (22). The resulting equation is eighth-order in the radial derivative and unsuitable for WKB analysis. However, we can determine the radial scale as $j' \to \infty$ by dimensional analysis, taking $\nabla^2 \sim \partial^2/\partial r^2 \sim 1/\Delta r^2$ and solving algebraically. This is the same procedure used to obtain equation (21). Formally treating Δr as a small parameter, we account for the fact that the diffusion coefficients have different scalings with respect to Δr, based on different numbers of radial derivatives operating on quantities within the coefficients. Arbitrarily taking $D_{nn}^{(2)}$ as a reference diffusion coefficient, the definitions in the Appendix show that if we define $D_{n\psi}^{(1)} = \Delta r d_{n\psi}^{(1)}$, $D_{n\psi}^{(2)} = (\Delta r)^3 d_{n\psi}^{(2)}$, $D_{nn}^{(1)} = (\Delta r)^2 d_{nn}^{(1)}$, $D_{nn}^{(2)} = d_{nn}^{(2)}$, $D_{\psi\psi} = (\Delta r)^2 d_{\psi\psi}$, and $D_{\psi n} = \Delta r d_{\psi n}$, then the lowercase diffusivities $d_{n\psi}^{(1)}$, $d_{n\psi}^{(2)}$, $d_{nn}^{(1)}$, $d_{nn}^{(2)}$, $d_{\psi\psi}$, and $d_{\psi n}$ are all of the same order. We formally order the large parameter j' by taking $mj' \to mj'/\epsilon$ and $\hat{\gamma} \to \hat{\gamma}/\epsilon$, where the controlling asymptotic limit becomes $\epsilon \to 0$. The relationship between ϵ and Δr will be derived by requiring that the asymptotic balance be consistent. After all leading-order expressions are derived, ϵ is set equal to 1.

Substituting these relations into equations (22) and (23) and solving, we obtain

$$\left\{ \frac{\epsilon^4}{\Delta r^4}[d_{\psi\psi}(d_{nn}^{(1)} + d_{nn}^{(2)}) - d_{\psi n}(d_{n\psi}^{(1)} + d_{n\psi}^{(2)})] - \frac{\epsilon^2}{\Delta r^2}[imj'(d_{n\psi}^{(1)} + d_{n\psi}^{(2)} + d_{\psi n}) - \gamma(d_{nn}^{(1)} + d_{nn}^{(2)} - d_{\psi\psi})] + m^2 j'^2 + \hat{\gamma}^2 \right\} \tilde{\psi}_{m,\gamma}^{(i)} = \left(\hat{\gamma} - \frac{d_{nn}^{(1)} + d_{nn}^{(2)}}{\Delta r^2} \right) S_\psi + (imj' + d_{\psi n})\Delta r S_n, \quad (28)$$

where

$$S_n = \frac{im}{r_0}\tilde{\psi}_{m,\gamma}\frac{d}{dr}J_0(r), \qquad S_\psi = \frac{im}{r_0}\tilde{\psi}_{m,\gamma}\frac{d}{dr}n_0(r) \quad (29)$$

are the turbulence sources described in the previous section. The left-hand side is a dimensional representation of a Green's function operator that governs the response to the sources. The spatial response decays inward from the edge of the filament where both the sources and the shear in B_θ are strong. Consequently, the field $\tilde{\psi}_{m,\gamma}$ appearing in the sources S_n and S_ψ is understood to be characteristic of the filament edge, and therefore ambient turbulence, while $\tilde{\psi}_{m,\gamma}^{(i)}$ is a response accounting for the refractive decay inside the filament. The scale length of the response Δr is found by solving the homogeneous problem, that is, by setting the left-hand side equal to zero and solving for Δr. In the limit $\epsilon \to 0$, turbulence remains in the dynamics and contributes to Δr only if $\epsilon \sim \Delta r$. Otherwise, the dynamics is laminar. The solution for Δr is

$$\left(\frac{\epsilon}{\Delta r}\right)^2 = \frac{imj'\hat{d}_2 - \hat{\gamma}\hat{d}_3}{2\hat{d}_1^2} + \frac{1}{2\hat{d}_1^2}[(imj'\hat{d}_2 - \hat{\gamma}\hat{d}_3)^2 - 4\hat{d}_1^2(m^2 j'^2 + \hat{\gamma}^2)]^{1/2}, \quad (30)$$

where $\hat{d}_1^2 = d_{\psi\psi}(d_{nn}^{(1)} + d_{nn}^{(2)}) - d_{\psi n}(d_{n\psi}^{(1)} + d_{n\psi}^{(2)})$, $\hat{d}_2 = d_{n\psi}^{(1)} + d_{n\psi}^{(2)} + d_{\psi n}$, and $\hat{d}_3 = d_{nn}^{(1)} + d_{nn}^{(2)} - d_{\psi\psi}$. This is the Alfvénic generalization of equation (21). It is more complicated but gives identical scaling. Recalling that all the lowercase diffusivities have the same scaling and replacing them with a generic d, the solution scales as $\epsilon^2/\Delta r^2 \sim mj'/d$. Setting $\epsilon = 1$,

$$\Delta r \sim \sqrt{d/mj'} \qquad (j' \to \infty). \quad (31)$$

The generic diffusivity d can be evaluated from the definitions given for specific diffusivities in the Appendix. If the turbulent decorrelation functions are evaluated in a strong-turbulence regime (turbulence timescales much shorter than linear timescales), then $d \sim \tilde{\psi}_m/a$, reproducing equation (21).

4.3. *Boundary-Layer Structure of Turbulence*

Although the structure function has not been solved (just its radial scale), its form in simpler cases illustrates the rapid decay of turbulence across the boundary layer, from the edge inward. Where WKB analysis is possible, the leading-order spatial Green's function has the form

$$G(r \mid r') \sim \exp\left[-C\left(\frac{r_< - r_0}{\sqrt{d/mj'}}\right)^\alpha\right]\exp\left[C\left(\frac{r_> - r_0}{\sqrt{d/mj'}}\right)^\alpha\right], \quad (32)$$

where C is a complex constant with positive real part, $r_<$ ($r_>$) is the smaller (larger) of r and r', and α is a positive constant determined by the order of the homogeneous operator. Here our dimensional solution of the problem, carried out by inverting equation (28), captures the radial integral over a structure function like that of equation (32). Solving equation (28), we obtain

$$\tilde{\psi}_{m,\gamma}^{(i)} \sim \hat{\gamma}^{-2}\left[\left(\hat{\gamma} - \frac{d_{nn}^{(1)} + d_{nn}^{(2)}}{\Delta r^2}\right)S_\psi + (imj' + d_{\psi n})\Delta r S_n\right] \sim \hat{\gamma}^{-1}\frac{m}{a}\tilde{\psi}_{m,\gamma}(r_0)(n_0' + \Delta r J_0'). \quad (33)$$

The temporal and spatial response to turbulent sources S_ψ and S_n at a point r_0 in the filament edge appears here as a structure factor of magnitude $\hat{\gamma}^{-2}$ multiplying the source. The product of source and response yields the value of $\tilde{\psi}^{(i)}$ inside the boundary layer. Beyond Δr

the response decays with an envelope like that of equation (32). The part of the source proportional to n_0' is essentially larger than the part proportional to J_0' by $O(a/\Delta r)$. However, if $\tilde{\psi}^{(i)}$ is substituted into the correlations of the equation for ψ_0 (eq. [11]), the J_0' part yields the diagonal terms. The density is given by the dimensional representation of equation (22),

$$\tilde{n}^{(i)}_{m,\gamma} \sim -\left(imj'\Delta r + \frac{d_{\psi n}}{\Delta r}\right)^{-1}\left(S_\psi + \frac{D_{\psi\psi}}{\partial r^2}\tilde{\psi}_{m,\gamma} - \hat{\gamma}\tilde{\psi}_{m,\gamma}\right) \sim \frac{\tilde{\psi}_{m,\gamma}(r_0)(n_0' + \Delta r J_0')}{aj'\Delta r}. \tag{34}$$

4.4. *Condition for Strong Refraction*

The layer width Δr is both the embodiment of the strong refraction of turbulent KAW activity in the filament by the large magnetic field shear j' and a condition for the refraction to be sufficiently strong to modify the scales of turbulence in the filament relative to those outside it. With a the scale of typical fluctuations of interest, the refraction is strong when $\Delta r/a \ll 1$, or

$$\frac{\Delta r}{a} \sim \sqrt{\frac{d|_{r>a}}{a^2 mj'}} \sim \sqrt{\frac{\tilde{\psi}|_{r>a}}{a^3 mj'}} \ll 1. \tag{35}$$

As a condition for strong refraction, it makes sense to use values for d or ψ that are typical of the turbulence in regions $r > a$, where there are no intense filaments. Inside a strong filament, the reduction of turbulent KAW activity represented by the structure factor $\hat{\gamma}^{-2}$ makes $d|_{r<a} \ll d|_{r>a}$. Accordingly, the boundary-layer width $\Delta r/a$ is smaller than $(d|_{r>a}/a^2 mj')^{1/2}$.

5. FILAMENT DECAY FROM MIXING STRESSES

The long time evolution of the filament fields $\psi_0(\tau)$ and $n_0(\tau)$ is governed by the mixing stresses of equations (11) and (12). These can now be evaluated using the boundary-layer responses $\tilde{\psi}^{(i)}_{m,\gamma}$ and $\tilde{n}^{(i)}_{m,\gamma}$ derived in the previous section. Because these fields are confined to the layer, the timescale τ is a mixing time across the boundary layer. For the diagonal stress components, the mixing is diffusive. The asymptotic behavior of the boundary layer yields the following dimensional equivalents: $r - r_0 \sim \Delta r$ and $\partial/\partial r \sim 1/\Delta r$, as before; $\int dr \sim \Delta r$; $\int d\gamma \sim mj'$; $\tilde{\psi}_{m,\gamma} \sim \psi_m(t)/mj'|_{t=0}$; and $\int d\gamma' \langle \tilde{\psi}\tilde{n}\rangle \sim \psi(t)n(t)/mj'|_{t=0}$. (The latter two expressions are inverse Laplace transform relations.) With these conventions,

$$\begin{aligned}\frac{\partial \psi_{\gamma=0}(\tau)}{\partial \tau} \approx \frac{\psi_{\gamma=0}}{\tau_\psi} = -\frac{1}{2\pi i}\int_{-i\infty+\gamma_0}^{+i\infty+\gamma_0} d\gamma' \sum_{m'}\Bigg[\frac{im'}{r}\left(\left\langle \tilde{\psi}^{(i)}_{-m',-\gamma'}\frac{\partial}{\partial r}\tilde{n}_{m',\gamma'}\right\rangle + \left\langle \tilde{\psi}_{-m',-\gamma'}\frac{\partial}{\partial r}\tilde{n}^{(i)}_{m',\gamma'}\right\rangle\right) \\ + \left(\left\langle \frac{\partial}{\partial r}\tilde{\psi}^{(i)}_{-m',-\gamma'}\tilde{n}_{m',\gamma'}\right\rangle + \left\langle \frac{\partial}{\partial r}\tilde{\psi}_{-m',-\gamma'}\tilde{n}^{(i)}_{m',\gamma'}\right\rangle\right)\frac{im'}{r}\Bigg] \\ \approx \sum_m \frac{1}{a^2 j'^2}(\langle \tilde{b}_{\theta-m}\tilde{n}_m\rangle|_{t=0} + \langle \tilde{b}^2_{\theta m}\rangle|_{t=0})(n_0' + \Delta r J_0'),\end{aligned} \tag{36}$$

where $\tilde{b}_{\theta m} = \tilde{\psi}_m/\Delta r$. The factor j'^{-2} in the rightmost form makes τ_ψ large; that is, mixing across the boundary layer is impeded by refraction. The turbulent fields in these expressions are filament-edge fields, that is, they are characteristic of ambient turbulence. The mixing time for current can be obtained by operating with ∇^2 on both sides of equation (36). On the left-hand side $\nabla^2\psi_{\gamma=0} \to \psi_{\gamma=0}/a^2$, while on the right-hand side $\nabla^2 \to 1/\Delta r^2$. Consequently,

$$\frac{\psi_{\gamma=0}}{\tau_J} \approx \sum_m \frac{1}{\Delta r^2 j'^2}(\langle \tilde{b}_{\theta-m}\tilde{n}_m\rangle|_{t=0} + \langle \tilde{b}^2_{\theta m}\rangle|_{t=0})(n_0' + \Delta r J_0'). \tag{37}$$

This timescale is much shorter because current, as a second derivative of ψ, has finer scale structure. If the filament is Alfvénic, that is, $n_0 \approx aJ_0$, the mixing time is dominated by the part of equation (37) that is proportional to n_0'. This represents off-diagonal transport of current driven by density gradient. The diagonal transport (driven by J_0') is current diffusion and is slower by a factor $a/\Delta r$. In the discussions that follow, we will deal with the current diffusion timescale, although similar behavior will hold for the off-diagonal transport. The mixing time for density is

$$\frac{\partial n_{\gamma=0}(\tau)}{\partial \tau} \approx \frac{n_{\gamma=0}}{\tau_n} \approx \sum_m \frac{2\langle \tilde{b}^2_{\theta m}\rangle|_{t=0}}{a^2 j'^2}\left(\frac{n_0'}{\Delta r} + J_0'\right). \tag{38}$$

Here the dominant component (proportional to n_0') is diffusive.

We evaluate these boundary-layer mixing times relative to the two turbulent timescales of the system. These are γ^{-1}, the turbulent decay time in the layer, and $\tau_A = a^2/\tilde{b}_\theta|_{r\gg a}$, a turbulent Alfvén time outside the filament. To simplify expressions, we note that Alfvénic equipartition implies that $\langle \tilde{b}_\theta \tilde{n}\rangle \approx \langle \tilde{b}^2_\theta\rangle$. We also note that $\psi_{\gamma=0}$ is in the Laplace-transform domain, whereas n_0' and J_0' are in the time domain. Under the inverse Laplace transform, $\psi_{\gamma=0}\gamma \approx \psi(t, \tau) \equiv \psi_0$. The scale of the filament is a, so $\psi_{\gamma=0}\gamma \approx a^2 J_0$. Similarly, $n_0' \approx n_0/a$, $J_0' \approx J_0/a$, and $j' = \partial/\partial r(B_\theta/r) \approx B_\theta/a^2$. We assume the filament is Alfvénic, making $n_0 \approx aJ_0$. With these relations,

$$\tau_n\gamma = \tau_{\nabla^2\psi}\gamma = \frac{\Delta r}{a}\frac{B_\theta^2}{\tilde{b}_\theta^2} \sim \left(\frac{a}{\Delta r}\right)^3 \sim \left(\frac{B_\theta}{\tilde{b}_\theta}\right)^{3/2}. \tag{39}$$

The last two equalities make use of equation (35) and the fact that $\Delta r/a$ and the mixing fluctuations are referenced to ambient turbulence levels for which $\tilde{b}_\theta \sim \tilde{\psi}/a \sim \tilde{b}_r$. Equation (39) indicates that turbulent diffusion times across the mixing layer Δr for both n_0 and J_0 are comparable and are much longer than the decay times of turbulence in the layer. The strong-shear limit, previously indicated by $j' \to \infty$, is here replaced by $B_\theta \to \infty$, because with a fixed radius a strong shear means large B_θ. In terms of τ_A,

$$\frac{\tau_n}{\tau_A} = \frac{\tau_{\nabla^2\psi}}{\tau_A} = \frac{\Delta r}{a}\frac{B_\theta}{\tilde{b}_\theta} \sim \frac{a}{\Delta r} \sim \left(\frac{B_\theta}{\tilde{b}_\theta}\right)^{1/2}, \tag{40}$$

indicating that these diffusion times are longer than the Alfvénic time of the ambient turbulence.

Either of the above expressions indicates that the actual lifetime of a filament (as opposed to the turbulent diffusion time across the edge layer) is virtually unbounded, provided that direct damping due to resistivity or collisional diffusion is negligible. During a filament lifetime, turbulence must diffuse across the scale a, many Δr-layer widths from the filament edge of to its center. However, in just a layer time τ_n or $\tau_{\nabla^2\psi}$, the turbulence is reduced by many factors of e^{-1}, while the filament density or current inside the layer remains untouched. Consequently, the width of the mixing layer at the edge of the filament continuously decreases even as the time to mix across it increases. The result is that mixing never extends to the filament core. This analysis shows that structures identified in the simulations as current filaments correlate spatially with a coherent density field, provided the density component is not destroyed by strong collisional diffusion.

6. GEOMETRIC AND STATISTICAL PROPERTIES

The above analysis treats the current of the filament as localized. The current is maximum at $r = 0$ and becomes zero at $r = a$. This makes the shear of the filament magnetic field largest in the filament edge and zero in the center. If it is true that the shear of this field refracts turbulent KAW activity as described above, turbulence is suppressed where the shear is large. These properties are incorporated in the spatial variation of a single quantity known as the Gaussian curvature (Terry 2000). The Gaussian curvature is a property of vector fields that quantifies the difference between shear stresses and rotational behavior. In rectilinear coordinates, the Gaussian curvature C_T of a vector field $\boldsymbol{A}(x, y)$ is

$$C_T = \left(\frac{\partial A_x}{\partial x} - \frac{\partial A_y}{\partial y}\right)^2 + \left(\frac{\partial A_y}{\partial x} + \frac{\partial A_x}{\partial y}\right)^2 - \left(\frac{\partial A_y}{\partial x} - \frac{\partial A_x}{\partial y}\right)^2 \tag{41}$$

(McWilliams 1984). For the total magnetic field in our cylindrical system, this can be written

$$C_T = \left[r\frac{d}{dr}\left(\frac{\tilde{b}_r}{r}\right) - \frac{1}{r}\frac{\partial}{\partial\theta}\tilde{b}_\theta\right]^2 + \left[r\frac{d}{dr}\left(\frac{B_\theta + \tilde{b}_\theta}{r}\right) + \frac{1}{r}\frac{\partial}{\partial\theta}\tilde{b}_r\right]^2 - (J_0 + \tilde{\jmath})^2. \tag{42}$$

Inside the filament, turbulence is suppressed and C_T is dominated by the filament field components B_θ and J_0. Near the center, J_0 is maximum and $d(B_\theta/r)/dr = j'$ vanishes, making C_T negative. Toward the filament edge, j' becomes maximum as J_0 goes to zero, making C_T positive. Outside the filament C_T is governed by $\tilde{b}_\theta$, $\tilde{b}_r$, and $\tilde{\jmath}$. These components must be roughly in balance. If they are not, the conditions for forming a coherent filament are repeated, and a structure should be present. Therefore, in regions where there are coherent filaments the Gaussian curvature should have a strongly negative core surrounded by a strongly positive edge. Where there are no coherent structures, the Gaussian curvature should be small. If this property is observed in simulations, it confirms the hypothesis that shear in the filament field refracts turbulent KAW activity in such a way as to suppress turbulent mixing of the structure. We note that the negative-core/positive-edge structure is predicted for current filaments of either sign, positive or negative. This type of Gaussian curvature structure has been observed in recent simulations (Smith & Terry 2006).

If the current filaments are well separated, their slow evolution relative to the decaying turbulence that surrounds them leads to a highly non-Gaussian PDF. Assuming an initial PDF that is Gaussian with variance $\langle J_\sigma^2\rangle$,

$$P(J) = \frac{1}{\sqrt{2\pi}\langle J_\sigma^2\rangle^{1/2}}\exp\left(\frac{-J^2}{2\langle J_\sigma^2\rangle}\right), \tag{43}$$

it is possible to model subsequent evolution on the basis of the timescales derived previously and the condition for strong refraction, equation (35). This condition stipulates that structures form where refraction is large, that is, where $mj' \gg \tilde{\psi}|_{r>a}/a^3$. Since $j' \approx J_0/a$ and $\tilde{\psi}|_{r>a}/a^2 \approx \langle J_\sigma^2\rangle^{1/2}$, structures occur for $J_0 \geq J_c = C\langle J_\sigma^2\rangle^{1/2}$, where C is the smallest numerical factor above unity to guarantee strong refraction and suppression of mixing. Given the latter, filaments reside on the tail of the PDF with high J and low probability $\int_{J_c}^{\infty} P(J)dJ$. This probability is equal to the filament packing fraction, that is, the fraction of 2D space occupied by current filaments. If, for simplicity, we assume that all filaments are of radius a, the faction of 2D space they occupy is $(a/l)^2$, where l is the mean distance between filaments. Therefore,

$$\int_{-\infty}^{-J_c} P(J)dJ + \int_{J_c}^{\infty} P(J)dJ = 2\int_{J_c}^{\infty} P(J)dJ = \left(\frac{a}{l}\right)^2, \tag{44}$$

where we assume that $P(J)$ is an even function. This expression gives the packing fraction as a function of the critical current J_c for filament formation.

It is now straightforward to construct a heuristic model for the evolution from the initial distribution. The model applies for times that are larger than the turbulent Alfvén time but shorter than the mean time between filament mergers. (Once filaments begin merging, their number and probability begin decreasing.) Prior to that time, the filament part of the distribution with $J > J_c$ is essentially unchanged, apart from the minor effects of slow erosion at the edge of the filaments. The probability that a fluctuation is not a filament also remains fixed, but these fluctuations decay in time. This means that the variance decreases while the probability remains fixed. The rate of decay is the turbulent Alfvén time τ_A. Therefore the distribution can be written

$$P(J,t) = \begin{cases} \dfrac{N(t)}{\sqrt{2\pi}\langle J_\sigma^2\rangle^{1/2}} \exp\left[\dfrac{-J^2}{2\langle J_\sigma^2\rangle \exp(-t/\tau_A)}\right] & \text{for } J < J_c, \\ \dfrac{1}{\sqrt{2\pi}\langle J_\sigma^2\rangle^{1/2}} \exp\left(\dfrac{-J^2}{2\langle J_\sigma^2\rangle}\right) & \text{for } J \geq J_c, \end{cases} \tag{45}$$

where $\langle J_\sigma^2\rangle$ remains the initial variance and $N(t)$ is a time-dependent normalization constant that maintains $\int_0^{J_c} P(J,t)dJ$ at its initial value, that is,

$$N(t) = \frac{\int_0^{J_c} dJ \exp(-J^2/2\langle J_\sigma^2\rangle)}{\int_0^{J_c} dJ \exp[-J^2 \exp(t/\tau_A)/2\langle J_\sigma^2\rangle]}. \tag{46}$$

The distribution $P(J, t)$ becomes highly non-Gaussian as $t \gg \tau_A$ because one part of the distribution (for $J < J_c$) collapses onto the $J = 0$ axis and becomes a delta function $\delta(J)$, while the other part remains fixed.

A simple measure of the deviation from a Gaussian distribution is the kurtosis,

$$\kappa(t) = \frac{3\int J^4 P(J,t)dJ}{\left[\int J^2 P(J,t)dJ\right]^2}. \tag{47}$$

The evolving kurtosis can be calculated directly from equation (45). While the exact expression is not difficult to obtain, its asymptote is more revealing. The kurtosis diverges from the initial Gaussian value of 3 as the contribution from turbulent kinetic Alfvén waves ($J < J_c$) decays and collapses to $\delta(J)$. After a few Alfvén times, the kurtosis is dominated by the part with $J > J_c$, which, because it is stationary, represents the time-asymptotic value for $\tau_A < t < \tau_M$. The time τ_M is the mean time to the first filament mergers. The time-asymptotic kurtosis is

$$\kappa(\tau_A \ll t \ll \tau_M) = \frac{6\int_{J_c}^{\infty} P(J)J^4\,dJ}{\left[2\int_{J_c}^{\infty} P(J)J^2\,dJ\right]^2} = \frac{3}{2}\left(\frac{l}{a}\right)^2\left[1 + \frac{\langle J_\sigma^2\rangle}{J_c^2} + O\left(\frac{\langle J_\sigma^2\rangle^{3/2}}{J_c^3}\right)\right]. \tag{48}$$

In writing this expression, the left-hand side of equation (44) has been expanded for $J_c^2 > \langle J_\sigma^2\rangle$ to yield $\langle j_\sigma^2\rangle \exp(-J_c^2/2\langle J_\sigma^2\rangle) = (a/l)^2 J_c[1 + O(\langle J_\sigma^2\rangle^{3/2}/J^3)]$. The time-asymptotic kurtosis is much greater than the initial Gaussian value of 3 and is characterized by the initial value of the inverse packing fraction. Once filament mergers begin, the inverse packing fraction increases above the initial value $(l/a)^2$. If $[l(t)/a]^2$ is the inverse packing fraction for $t > \tau_M$, the above analysis suggests that the kurtosis will continue increasing as $(3/2)[l(t)/a]^2$ for late times.

We now consider the distribution of density. As shown in the previous section, the density present in the current filament also has suppressed mixing and is therefore coherent, or long-lived. However, it is not spatially intermittent to the same degree as the current. Alfvénic dynamics indicate that $n \approx B$, while Ampère's law stipulates that the magnetic field of the filament extends into the region $r > a$, falling off as r^{-1}. Hence the density associated with filaments also is expected to fall off as r^{-1} for $r > a$. This spatially extended structure makes density less isolated than current. It produces higher probabilities for low values of density than those of decaying turbulence. This will yield a kurtosis closer to the Gaussian value of 3 than the kurtosis of the current. However, the distribution of low-level density associated with the structure likely will not be Gaussian. It is ultimately the distribution that matters for the scattering of radio-frequency (RF) pulsar signals.

To construct the density PDF, we seek the mapping of density onto the spatial area it occupies. We obtain this mapping for the filament density, assuming that the density of turbulence is low and has effectively collapsed onto $n = 0$ after a few τ_A, just as the current. The density for $r > a$ varies as $n = an_0/r$, where n_0 is the value of the density at $r = a$. As shown in Figure 3, the area occupied for a given density is $2\pi r\,dr$. This area is the probability when properly normalized; hence,

$$P(n)dn = 2\pi r\,dr. \tag{49}$$

Writing $r\,dr$ in terms of n and dn using $n = an_0/r$, $P(n) = C_n/n^3$, where C_n is the normalization constant chosen so that the probability integrated over the whole filament with its r^{-1} mantle equals the packing fraction, or probability of finding the filament in some sample area. With the long, slowly decaying tail of n^{-3} it is necessary to impose a cutoff to keep the PDF integrable. The cutoff, which we label n_c, corresponds to the low level of decaying turbulence but otherwise need not be specified. Consequently, the normalization is determined by

$$2C_n \int_{n_c}^{n_0} \frac{dn}{n^3} = \begin{cases} (r_c/l)^2, & \text{for } r_c < l, \\ 1, & \text{for } r_c \geq l, \end{cases} \tag{50}$$

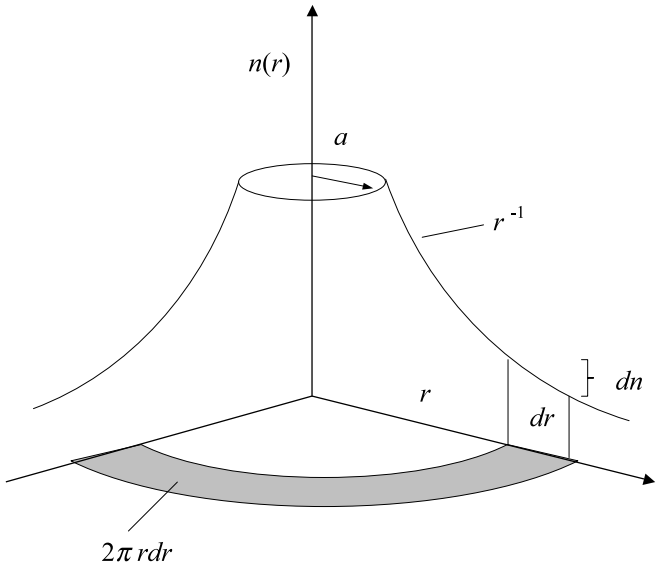

FIG. 3.—The probability of density outside $r = a$ maps onto the annular area $2\pi r\,dr$.

where r_c, the radius at which $n = n_c$, is $r_c = an_0/n_c$. The first of the two possibilities in equation (50) allows for a cutoff radius that is smaller than the mean distance between structures (of radius r_c), yielding a probability that is less than unity. If the cutoff radius is equal to or larger than the mean separation, then the structures are space-filling and the probability is unity. Solving for C_n, the normalized density PDF is

$$P(n) = \begin{cases} \dfrac{a^2}{l^2}\dfrac{n_0^4}{(n_0^2 - n_c^2)n^3}, & \text{for } r_c < l \text{ or } \dfrac{a}{l} < \dfrac{n_c}{n_0}, \\ \dfrac{n_0^2 n_c^2}{(n_0^2 - n_c^2)n^3}, & \text{for } r_c \geq l \text{ or } \dfrac{a}{l} \geq \dfrac{n_c}{n_0}. \end{cases} \tag{51}$$

This distribution is defined for $n_c < n < n_0$. It captures only the contribution of filaments and ignores the density inside $r = a$, which makes a small contribution to the PDF.

This distribution is certainly non-Gaussian, because it has a tail that decays slowly as n^{-3}. However, depending on the length of the tail, which is set by n_c and n_0, the distribution may or may not deviate from a Gaussian in a significant way over $n_c < n < n_0$. This is quantified by the kurtosis,

$$\kappa(n_0, n_c) = \frac{6C_n \int_{n_c}^{n_0} n^4 (n^{-3}\,dn)}{C_n^2 [2\int_{n_c}^{n_0} n^2 (n^{-3}\,dn)]^2}. \tag{52}$$

Substituting from equation (51), we find that

$$\kappa(n_0, n_c) = \begin{cases} \dfrac{3}{4}\dfrac{l^2}{a^2}\dfrac{1 - 2n_c^2/n_0^2 + n_c^4/n_0^4}{[\ln (n_0/n_c)]^2}, & \text{for } r_c < l \text{ or } \dfrac{a}{l} < \dfrac{n_c}{n_0}, \\ \dfrac{3}{4}\dfrac{n_0^2}{n_c^2}\dfrac{1 - 2n_c^2/n_0^2 + n_c^4/n_0^4}{[\ln (n_0/n_c)]^2}, & \text{for } r_c \geq l \text{ or } \dfrac{a}{l} \geq \dfrac{n_c}{n_0}. \end{cases} \tag{53}$$

These expressions are smaller than the current kurtosis by a factor $2[\ln (n_0/n_c)]^2$. Unless n_0/n_c is quite large, the kurtosis may not rise significantly above 3. This is particularly true in simulations with limited resolution, where dissipation will affect the density, either directly through a collisional diffusion or indirectly by resistive diffusion of current filaments. Kurtosis increases if n_c decreases. However, while n_c is tied to the decreasing turbulence level, regeneration of the turbulence by the r^{-1} mantle may prevent n_c from becoming very small. Nonetheless, mergers of filaments will decrease the packing fraction. Even if the density is space-filling initially and satisfies the second possibility in equation (53), the mean filament separation will increase above r_c at some point, and the kurtosis will be given by the first possibility. Then as the inverse packing fraction increases above l^2/a^2, the kurtosis will rise.

The n^{-3} falloff of the density PDF has intriguing implications for RF scattering of pulsar signals. Noting that the scattering is produced by gradients of density, the extended density structure for $r > a$ yields $\nabla n \equiv n' \sim 1/r^2$. We can construct the PDF for n' following the procedure used for the PDF of n. Writing rdr in terms of n' and dn' using $r \sim (n')^{-1/2}$, we recover

$$P(n') = C_{n'}/(n')^2, \tag{54}$$

where $C_{n'}$ is a constant. This is a Levy distribution, the type of distribution inferred in the scaling of pulsar signals (Boldyrev & Gwinn 2003a). Further exploration of the implications of these results to RF scattering of pulsar signals remains an important question for future work.

7. CONCLUSIONS

We have examined the formation of coherent structures in decaying kinetic Alfvén wave turbulence to determine if there is a dynamical mechanism in interstellar turbulence that leads to a non-Gaussian PDF in the electron density. Such a PDF has been inferred from scalings in pulsar scintillation measurements. We use a model for kinetic Alfvén wave turbulence that is applicable when there is a strong mean magnetic field. The nonlinearities couple density and magnetic field in the plane perpendicular to the mean field in a way that is analogous to the coupling of flow and magnetic field in reduced MHD. The model applies at scales on the order of the ion gyroradius and smaller. We show that the coherent current filaments previously observed to emerge from a Gaussian distribution in simulations of this model (Craddock et al. 1991) result from strong refraction of turbulent kinetic Alfvén waves. The refraction occurs in the edge of intense, localized current fluctuations and is caused by the strongly sheared magnetic field associated with the current. This refraction localizes turbulent wave activity to the extreme edge of the filament and impedes mixing (turbulent diffusion) of the filament current by the turbulence. From this analysis, we conclude that the turbulence suppression by sheared flows common in fusion plasmas (Terry 2000) has a magnetic analog in situations where there is no flow. This leads to a further conclusion that intermittent turbulence, which is generally associated with flows, can occur in situations where there is no flow. (By flow we mean ion motion. Electron motion is incorporated in the current.) We have derived a condition for the strength of magnetic shear required to produce the strong refraction and suppress mixing. We show that this condition yields a prediction for the Gaussian curvature of the magnetic field. This quantity is predicted to have large values inside the coherent current filaments and small values everywhere else. Inside filaments, the Gaussian curvature is negative at the center and positive at the edge.

The analysis shows that long-lived fluctuation structures form in the density and magnetic field, provided damping is negligible. Like the current filaments, these structures avoid mixing because of the refraction of turbulent kinetic Alfvén wave activity. Hence they occur in the same physical location as the current filaments. However, the localized nature of the current filaments gives the long-lived magnetic field an extended region external to the current. In this region the field falls off as r^{-1}, where r is the distance from the center of the filament. Because kinetic Alfvén wave dynamics yields an equipartition of density and magnetic field fluctuations, we posit that the long-lived density has a similar extended structure. As a result, the connection between coherent structure and localization that is true for the current, and makes it highly intermittent, does not apply to the density. While there is coherent long-lived density, it need not be localized. A similar situation holds for vorticity and flow in 2D Navier-Stokes turbulence (McWilliams 1984). To explore this matter, we have used the physics of the coherent structure formation to derive heuristic probability distribution functions for the current and density. As the turbulence decays, leaving intense current fluctuations as coherent current filaments, the kurtosis of current increases to a value proportional to the packing fraction. The kurtosis of density does not become as large and could, under appropriate circumstances, remain close to the Gaussian value of 3. However, mergers of structures in a situation with very weak dissipation could increase the kurtosis well above 3. More importantly, however, the density PDF is non-Gaussian even when its kurtosis is not greatly different from 3. The r^{-1} structure external to the current gives the PDF a tail that varies as n^{-3}. Mapping the r^{-1} structure to a PDF in density gradient, the density gradient PDF decays as $1/n'^2$, a Levy distribution. This suggests that the mechanism described here may play a role in the scaling of pulsar RF signals.

Several aspects of this problem need additional study. It is important to adapt these results to a steady state. Generally speaking, there is a dynamical link between decaying turbulence and turbulence in a stationary dissipation range. Hence these results, at least qualitatively, are relevant to the dissipation range. Dissipation begins to affect the spectrum at a scale that is somewhat larger (an order of magnitude) than the nominal dissipation scale (Frisch 1995). Structures such as these would correspond to active, filamentary regions of dissipation analogous to those observed in neutral gas clouds, albeit at a much smaller scale and with no accompanying flow shear signature. Intermittent structures can extend into the stationary inertial range, but the analysis presented here must be modified. In the inertial range turbulence is replenished, allowing the slow mixing of a coherent structure to continue until it is gone. Structures are also regenerated by the turbulence, and the statistics is ultimately set by a balance of mixing and regeneration rates. The mixing rates calculated here are slow enough in strong filaments that coherent structure formation is expected even in a steady state. There is also a possible link between structures in the larger scale range of shear Alfvén excitations and KAW excitations. These questions will be explored in future work. While gyroradius-scale KAW turbulence may arise in astrophysical contexts other than the ISM, the small scales make it unlikely that astrophysical observations will be available for testing this theory. Therefore, simulations should be used to check key conclusions from the theoretical work presented here. These include the formation of density structures, which was not reported in Craddock et al. (1991), the structure of the Gaussian curvature, which validates the refraction hypothesis, and the existence of the r^{-1} structure in the density and its effect on the PDF. The effect of this type of density field on RF scattering remains the underlying question, and modeling of the scattering with simulated fields should be pursued.

The authors acknowledge useful conversations with Stanislav Boldyrev, including his observation that the density PDF derived herein immediately leads to a Levy distribution in the density gradient. P. W. T. also acknowledges the Aspen Center for Physics, where part of this work was performed. This work was supported by the National Science Foundation.

APPENDIX

Closures truncate the moment hierarchy that is generated when averages are taken of nonlinear equations. The closure we have used is of the eddy-damped quasi-normal Markovian variety and follows the steps of the closure calculation described in Terry et al. (2001).

The nonlinear decorrelation is calculated consistent with the statistical *Ansatz*, not imposed ad hoc. The closure equations are given in equations (22) and (23). The other diffusivities not given in equation (24) are

$$D_{\psi n}(m,\gamma)=\frac{1}{2\pi i}\int_{-i\infty+\gamma_0}^{+i\infty+\gamma_0}d\gamma'\sum_{m'\neq 0,m}\frac{m'}{r}\left[\left\langle\tilde{\psi}_{m',\gamma'}K_2(m-m',\gamma-\gamma')\Delta W_{\gamma,\gamma'}\frac{m'}{r}\psi_{-m',-\gamma'}\right\rangle+\left\langle\tilde{n}_{m',\gamma'}K_3(m-m',\gamma-\gamma')\Delta W_{\gamma,\gamma'}\frac{m'}{r}\psi_{-m',-\gamma'}\right\rangle\right],\tag{A1}$$

$$D^{(1)}_{nn}(m,\gamma)=\frac{1}{2\pi i}\int_{-i\infty+\gamma_0}^{+i\infty+\gamma_0}d\gamma'\sum_{m'\neq 0,m}\frac{m'}{r}\left[\left\langle\tilde{\psi}_{m',\gamma'}K_3(m-m',\gamma-\gamma')\Delta W_{\gamma,\gamma'}\frac{m'}{r}\psi_{-m',-\gamma'}\right\rangle\right],\tag{A2}$$

$$\begin{aligned}D^{(2)}_{nn}(m,\gamma)=\frac{1}{2\pi i}\int_{-i\infty+\gamma_0}^{+i\infty+\gamma_0}d\gamma'\sum_{m'\neq 0,m}\Bigg[&\frac{m'}{r}\left\langle\tilde{\psi}_{m',\gamma'}\nabla^2K_3(m-m',\gamma-\gamma')\Delta W_{\gamma,\gamma'}\frac{m'}{r}\psi_{-m',-\gamma'}\right\rangle\\&-\frac{m-m'}{r}\left\langle\frac{\partial\tilde{\psi}_{m',\gamma'}}{\partial r}K_3(m-m',\gamma-\gamma')\Delta W_{\gamma,\gamma'}\left(\frac{m}{r}\right)\frac{\partial\tilde{\psi}_{-m',-\gamma'}}{\partial r}\right\rangle\\&-\frac{m}{r}\left\langle K_3(m-m',\gamma-\gamma')\Delta W_{\gamma,\gamma'}\frac{m'}{r}\tilde{\psi}_{m',\gamma'}\nabla^2\tilde{\psi}_{-m',-\gamma'}\right\rangle\Bigg],\end{aligned}\tag{A3}$$

$$D^{(2)}_{n\psi}(m,\gamma)=\frac{1}{2\pi i}\int_{-i\infty+\gamma_0}^{+i\infty+\gamma_0}d\gamma'\sum_{m'\neq 0,m}\frac{m'}{r}\left[\left\langle\tilde{\psi}_{m',\gamma'}K_1(m-m',\gamma-\gamma')P^{-1}_{m-m'}\Delta W_{\gamma,\gamma'}\frac{m'}{r}\psi_{-m',-\gamma'}\right\rangle\right],\tag{A4}$$

$$\begin{aligned}D^{(1)}_{n\psi}(m,\gamma)=\frac{1}{2\pi i}\int_{-i\infty+\gamma_0}^{+i\infty+\gamma_0}d\gamma'\sum_{m'\neq 0,m}\Bigg[&\frac{m'}{r}\left\langle\tilde{\psi}_{m',\gamma'}K_1(m-m',\gamma-\gamma')\nabla^2P^{-1}_{m-m'}\Delta W_{\gamma,\gamma'}\frac{m'}{r}\tilde{\psi}_{-m',-\gamma'}\right\rangle\\&-\frac{m-m'}{r}\left\langle\frac{\partial\tilde{\psi}_{m',\gamma'}}{\partial r}K_1(m-m',\gamma-\gamma')P^{-1}_{m-m'}\Delta W_{\gamma,\gamma'}\left(\frac{m}{r}\right)\frac{\partial\tilde{\psi}_{-m',-\gamma'}}{\partial r}\right\rangle\\&+\frac{m}{r}\left\langle K_1(m-m',\gamma-\gamma')P^{-1}_{m-m'}\Delta W_{\gamma,\gamma'}\frac{m'}{r}\tilde{\psi}_{-m',-\gamma'}\nabla^2\tilde{\psi}_{m',\gamma'}\right\rangle\\&+\frac{m'}{r}\left\langle\tilde{\psi}_{m',\gamma'}K_1(m-m',\gamma-\gamma')P^{-1}_{m-m'}\Delta W_{\gamma,\gamma'}\frac{m'}{r}\nabla^2\tilde{\psi}_{-m',-\gamma'}\right\rangle\\&+\frac{m'}{r}\left\langle\tilde{\psi}_{m',\gamma'}K_3(m-m',\gamma-\gamma')\Delta W_{\gamma,\gamma'}\frac{m'}{r}\nabla^2\tilde{n}_{-m',-\gamma'}\right\rangle\Bigg],\end{aligned}\tag{A5}$$

where

$$K_2(m,\gamma)=-\left\{1-P_m^{-1}\left[\hat{\gamma}-D^{(1)}_{nn}(m,\gamma)\frac{\partial^2}{\partial r^2}\nabla_m^2-D^{(2)}_{nn}(m,\gamma)\frac{\partial^2}{\partial r^2}\right]\right\}\left[imj'(r-r_0)+D_{\psi n}(m,\gamma)\frac{\partial^2}{\partial r^2}\right]^{-1},\tag{A6}$$

$$K_3(m,\gamma)=K_1(m,\gamma)K_2(m,\gamma)+\left[-\hat{\gamma}+D_{\psi\psi}(m,\gamma)\frac{\partial^2}{\partial r^2}\nabla_m^2-\frac{im}{r}\frac{d}{dr}n_0\right]^{-1},\tag{A7}$$

and P_m and $K_1(m,\gamma)$ are given in equations (25) and (26). These expressions contain both linear wave terms and nonlinear diffusivities and are valid in both weak- and strong-turbulence regimes. Outside filaments, where turbulence levels are evaluated to derive the condition for strong refraction (eq. [35]), the turbulence is strong. The strong-turbulence limit of the above expressions yields the diffusivity d that appears in equation (35).

REFERENCES

Armstrong, J. W., Cordes, J. M., & Rickett, B. J. 1981, Nature, 291, 561
Armstrong, J. W., Rickett, B. J., & Spangler, S. R. 1995, ApJ, 443, 209
Bale, S. D., Kellogg, P. J., Mozer, F. S., Horbury, T. S., & Rème, H. 2005, Phys. Rev. Lett., 94, No. 215002
Bhat, N. D. R., Cordes, J. M., Camilo, F., Nice, D. C., & Lorimer, D. R. 2004, ApJ, 605, 759
Boldyrev, S., & Gwinn, C. 2003a, ApJ, 584, 791
Boldyrev, S., & Gwinn, C. R. 2003b, Phys. Rev. Lett., 91, No. 131101
Boldyrev, S., & Königl, A. 2006, ApJ, 640, 344
Craddock, G. G., Diamond, P. H., & Terry, P. W. 1991, Phys. Fluids B, 3, 304 (erratum 3, 1791)
Frisch, U. 1995, Turbulence (Cambridge: Cambridge Univ. Press)
Grappin, R., Velli, M., & Mangeney, A. 1991, Ann. Geophys., 9, 416
Hazeltine, R. D. 1983, Phys. Fluids, 26, 3242
Head, M. R., & Bandyopadhyay, P. 1981, J. Fluid Mech., 107, 297
Hily-Blant, P., Pety, P., & Falgarone, E. 2007, preprint (astro-ph/0701326)
Hof, B., et al. 2004, Science, 305, 1594
Howes, G. G., Cowley, S. C., Dorland, W., Hammett, G. W., Quataert, E., & Schekochihin, A. A. 2006, ApJ, 651, 590
Kerr, R. 1986, J. Fluid Mech., 153, 31
McWilliams, J. C. 1984, J. Fluid Mech., 146, 21
Politano, H., & Pouquet, A. 1995, Phys. Rev. E, 52, 636
She, Z.-S., & Lévêque, E. 1994, Phys. Rev. Lett., 72, 336
Smith, K., & Terry, P. 2006, Bull. Am. Phys. Soc., 51, 251
Sutton, J. M. 1971, MNRAS, 155, 51
Terry, P. W. 1989, Physica D, 37, 542
———. 2000, Rev. Mod. Phys., 72, 109
Terry, P. W., Fernandez, E., & Ware, A. S. 1998, ApJ, 504, 821
Terry, P. W., McKay, C., & Fernandez, E. 2001, Phys. Plasmas, 8, 2707
Terry, P. W., Newman, D. E., & Mattor, N. 1992, Phys. Fluids A, 4, 927
Waleffe, F. 1997, Phys. Fluids, 9, 883